Polarization-dependent Raman spectra of heteroepitaxial $(Ba,Sr)TiO_3/MgO$ thin films

Yu. I. Yuzyuk
Faculty of Physics, Rostov State University, Zorge 5, Rostov-on-Don 344090, Russia

V. A. Alyoshin, I. N. Zakharchenko, and E. V. Sviridov
Institute of Physics, Rostov State University, Stachki 194, Rostov-on-Don 344090, Russia

A. Almeida and M. R. Chaves
Departamento de Física, IFIMUP, Faculdade de Ciências da Universidade do Porto, Rua do Campo Alegre 687, 4169-007 Porto, Portugal

(Received 26 July 2001; revised manuscript received 23 October 2001; published 19 March 2002)

We have studied the concentration dependence of the Raman spectra of heteroepitaxial $(Ba_{1-x}Sr_x)TiO_3$ (BST) ($x=0$, 0.15, 0.30, and 0.45) thin films deposited by rf sputtering on (001) MgO substrates. It is found that substitution of Ba by Sr leads to the distortions of the Ti-O bonds and causes the appearance of new bands in the Raman spectra near the bands corresponding to the Ti-O vibrations. The Sr incorporation induces relatively large shifts of the low-frequency Raman peaks attributed to E_{TO} and $A_{1\,TO}$ components of the soft mode. The E_{TO} soft mode in BST films becomes underdamped for $x \geqslant 0.3$ and is very sensitive to the two-dimensional compressive stresses.

DOI: 10.1103/PhysRevB.65.134107 PACS number(s): 63.20.−e, 77.55.+f, 68.49.Uv

I. INTRODUCTION

Integrated thin-layer ferroelectrics have become very attractive as active elements in microelectronic devices. The structure and properties of thin films are well known to exhibit a number of deviations from those of bulk ceramics and single crystals. The origin of the size-dependent ferroelectric properties remains a challenging problem, and a better understanding as to which extent the bulk physical properties can be used for design of thin-layer devices is actually required. The bulk properties of ferroelectric $BaTiO_3$ (BT) and quantum paraelectric $SrTiO_3$ (ST) were extensively studied in the past; therefore, in addition to practical interest, thin films of their solid solutions are very attractive as model systems for studying the effect of finite size on ferroelectric properties.

Thin films of $(Ba_{1-x}Sr_x)TiO_3$ (BST-x) are very good candidates for a wide range of applications: for example, as high-density dynamic random access memories, large-scale integrated capacitors, pyroelectric detectors, and phase shifters.[1,2] High-quality BST epitaxial films are required for tunable microwave applications.[3] Therefore, the synthesis and characterization of BST thin films have generated large research efforts in the last few years. The optical, structural, and electrical properties of BST films have been found to depend substantially on the preparation method, composition, film thickness, grain size, and annealing.[4–7] Consequently, reliable methods to characterize thin films are of great interest.

Raman spectroscopy has been used as a nonperturbing probe for thin films characterization. Useful information about impurities, internal stress, and crystal symmetry has been obtained in various thin and ultrathin films.[8–13] Moreover, the structural changes associated with the ferroelectric phase transition usually have a large effect on the Raman spectrum. As known from the Lyddane-Sachs-Teller relation, the dramatic increase of the low-frequency dielectric constant ϵ_0 near T_c is directly related to the soft-mode behavior. It should be underlined that the soft-mode temperature dependence in thin ferroelectric films usually deviates from the values known for bulk single crystals.[10,14] Very recent far-infrared (FIR) ellipsometry and low-frequency dielectric measurements in ST thin films revealed that the dramatic reduction of the dielectric constant is a consequence of the soft-mode hardening.[15] In this aspect the lattice dynamics—in particular, the soft-mode behavior—is of great importance for the purpose of thin film characterization.

BT and ST are the classic and most studied ferroelectrics, both theoretically and experimentally.[16] In the paraelectric cubic phase BT and ST have similar crystal structure. Explicit first-principles calculations showed that the differences between BT and ST are to some extent volume effects, which are shown by a compression of BT unit cell to the volume of ST one or a dilatation of ST to the volume of BT.[17] A widely accepted view is that the lattice instability of BT stems from the Ti($3d$) and O($2p$) hybridization that prefers a smaller Ti-O distance than half of the lattice constant of BT.[17,18] Most of the experimental data obtained in BT are consistent with a complicated combination of displacive and order-disorder behavior. According to the order-disorder model, in the paraelectric phase the Ti ion does not have a potential energy minimum at the center of the unit cell, but has eight minima along the [111] pseudocubic axes. In the tetragonal phase, four sites along a face of the unit cell become energetically favored, with a time-averaged position along the c axis, in the orthorhombic phase the Ti ions preferentially occupy two of the eight sites, and finally in the rhombohedral phase they are completely ordered.[19] Within the framework of the displacive model, the atoms primarily occupy the ideal cubic sites at high temperatures and the ferroelectric F_{1u} soft-mode in BT corresponds to Ti displacement with respect to oxygen octahedra.[20,21]

Vibrational spectra of BT single crystals have been extensively studied in the past[22–27] and lend support to displacive-order-disorder crossover. No first-order Raman activity is expected in the paraelectric phase with ideal O_h^1 cubic symmetry, but two broad bands at ~ 260 and 530 cm^{-1} persist with significant intensity[22,23] due to disorder of Ti ions in agreement with eight-site model. The lowest-lying transverse F_{1u} mode exhibits softening in the paraelectric phase and supports the displacive mechanism. However, this mode is overdamped, apparently, due to the above-mentioned large amplitude motion (hopping) of the Ti ions. Furthermore, FIR reflectivity measurements[24] indicated that on cooling, the soft mode levels off near 60 cm^{-1} far above $T_c \sim 395$ K and it was emphasized that the soft mode is unable to explain the temperature dependence of ϵ_0 in the vicinity of T_c. Very probably the soft mode levels off due to its coupling with the critical relaxation, revealed from backward-wave-oscillator transmission measurements where its complete softening below 10 cm^{-1} was found, explaining the whole dielectric anomaly at the cubic-tetragonal phase transition in BT.[26]

In the tetragonal phase the soft mode splits into A_1 and E components. At room temperature, the E_{TO} soft mode is also overdamped and according to the results reported in numerous papers and summarized by Scalabrin *et al.*[23] the soft-mode frequency is about 34–38 cm^{-1}, while the half-width is somewhere between 85 and 115 cm^{-1}. This low-frequency response may be also well fitted even by a Debye relaxator. The corresponding A_1 component of the soft mode is found at about 276 cm^{-1}. In the orthorhombic phase the soft mode becomes underdamped and slightly softens with decreasing temperature, while at the transition to the rhombohedral phase this mode abruptly stiffens[27] up to 250 cm^{-1}.

Due to quantum fluctuations the ferroelectric state does not occur in pure ST, but ferroelectricity can be induced by stress, electric field, and doping. The ferroelectric F_{1u} soft mode in ST was revealed in the broad temperature interval 8–1200 K by FIR reflectivity,[28] neutron scattering,[29] and Raman scattering under applied electric field.[30] The soft mode is always underdamped and its frequency decreases from 150 cm^{-1} at 1200 K down to 11 cm^{-1} at 8 K. Although the ferroelectric F_{1u} soft mode explains rather well the temperature dependence of the dielectric constant and the displacive mechanism in ST dominates, we note that the displacive-order-disorder crossover has been found at the 105-K structural transition of ST involving the zone-boundary R_{25} mode related to the libration of the oxygen octahedra.[31]

Presently available information concerning the lattice dynamics of BST-x solid solutions is rather fragmental. Detailed concentration dependence of phonon-mode frequencies in BST-x ceramics at 6 K was reported,[32] but the temperature dependence was not studied. Later on, the soft-mode behavior in the powder sample of BST-0.5 was disclosed by neutron-diffraction measurements.[33] FIR measurements in paraelectric phase[34] revealed that the soft mode becomes underdamped in BST-0.1 bulk crystals, whereas room temperature FIR transmission spectra[35] of BST-x films ($x=0.35$ and 0.65) showed very broad absorption peaks above 100 cm^{-1}. The temperature dependence of unpolarized Raman spectra of bulk ceramics and polycrystalline films BST-x ($x=0$, 0.1, 0.2, and 0.3) in the range between room temperature and 350 °C was recently published by Naik *et al.*[13] but no evidence of the soft mode was found. It was reported that the values of T_c in thin films are higher than those of the bulk samples due to the presence of intergrain stress. Furthermore, a new Raman mode has been disclosed at ~ 620 cm^{-1} in all the thin-film samples. These authors proposed that this new mode originates from the strain in the grain-boundary regions of the polycrystalline film.

In our recent paper, polarization-dependent Raman spectra of BST-x/MgO ($x=0$ and 0.45) heteroepitaxial thin films were reported for the first time.[36] The underdamped E_{TO} soft mode centered at 89 cm^{-1} at room temperature was unambiguously observed in the film with $x=0.45$. It is puzzling that the temperature dependence of the E_{TO} soft mode in the BST-0.45 film is very similar to those previously reported for pure ST films.[14,15,37–40] Namely, the lowest E_{TO} mode exhibits softening down to ~ 100 K, but in contrast to the bulk ST, BT crystals, and BST-0.5 powder sample, this mode saturates at ~ 64 cm^{-1} on further cooling.

In this paper, we report the experimental results obtained from the heteroepitaxial thin-film samples of BST-x ($x=0$, 0.15, 0.30, and 0.45) prepared on MgO substrates. A detailed mode assignment and a comparison with bulk ceramics is given. The lattice dynamics is discussed in the terms of a displacive-order-disorder crossover, previously established in ferroelectric perovskites. We have considered the influence of several phenomena, which lead to profound changes in the Raman spectra of BST thin films with respect to bulk ceramics.

II. EXPERIMENTAL DETAILS

Heteroepitaxial BST-x (thickness 0.5–0.8 μm) thin films were deposited on (001) MgO single crystalline substrates by rf sputtering of polycrystalline targets of the corresponding composition. Transparent and mirror-smooth films were realized by means of layer-by-layer growth. Details of the growth conditions have been previously reported.[41–43] Briefly, the deposition [density of rf discharge $(1–2.5)\times 10^5$ W m^{-2}, target-substrate distance 6–10 mm] was carried out in oxygen atmosphere under a pressure of 0.6–0.7 Torr. The substrates were heated at 800–950 °C during the deposition. The film composition was determined by primary x-ray spectra, obtained on the CAMEBAX microanalyzer with an accuracy of $\pm 2\%$. The surface and cross-section relief (before and after chemical etching) of the films were studied by optical and electron microscopy. After etching, perfect BST films displayed well-defined 180° c-domain structure.[44] The unit-cell parameters at room temperature were determined by means of x-ray diffraction (XRD) and summarized in Table I. For all the films studied here, a tetragonal distortion with the c axis perpendicular to the substrate and the following orientation relations between the BST-x film and the MgO substrate have been found: $(001)_{BST} \| (001)_{MgO}$ and $[100]_{BST} \| [100]_{MgO}$. For temperature-dependent measurements, the DRON-3 dif-

TABLE I. Lattice parameters, c/a ratio and the soft-mode frequency for the BST-x films studied in the present work. Raman spectra of the films, which are marked by asterisks in the left column, are shown in Figs. 1–3.

Sr concentration, x	c (Å)	a (Å)	c/a ratio	E_{TO} soft-mode frequency (cm^{-1})
0*	4.0318	3.998	1.008	35±5 overdamped
0.15*	4.0190	3.978	1.010	45±5 overdamped
0.30	3.9888	3.969	1.005	56±2
0.30	3.9956	3.959	1.009	60±1
0.30*	4.0001	3.954	1.012	68±1
0.30	4.0065	3.957	1.013	79±1
0.45*	3.991	3.939	1.013	83±1

fractometer was supplied with a precise heater with a temperature stability ±0.5 K.

Raman spectra were excited using the polarized light of a coherent INNOVA 90 Ar^+ laser ($\lambda = 514.5$ nm) and analyzed using a Jobin Yvon T64000 spectrometer equipped with a charge coupled device and a photon counting detector. Polarization-dependent Raman spectra have been measured on samples carefully oriented according to the crystallographic axes of c-domain films: $X \| [100]$, $Y \| [010]$, and $Z \| [001]$. Raman spectra were obtained in backscattering geometry using a microprobe device that allows the incident light to be focused on the sample as a spot of about 2 μm in diameter. For high-temperature measurements the samples were placed in a hot stage where the temperature was controlled with accuracy better than 0.2 K.

III. EXPERIMENTAL RESULTS

In the paraelectric cubic phase of ABO_3 perovskites there are 12 optic modes that transform according to the triply degenerate irreducible representations of the O_h point group: $\Gamma_{cub} = 3F_{1u} + F_{2u}$. The F_{1u} modes are IR active and the F_{2u} is the so-called ''silent mode'' since it is neither IR nor Raman active. In the tetragonal ferroelectric phase, each triply degenerate F_{1u} mode splits into $A_1 + E$ modes, while the F_{2u} silent mode splits into $B_1 + E$ modes. Thus, $\Gamma_{tet} = 3A_1 + 4E + B_1$. All the A_1 and E modes are both IR and Raman active while the B_1 mode is only Raman active. In addition, long-range electrostatic forces in the ferroelectric phase split all the A_1 and E modes into transverse (TO) and longitudinal (LO) components. Detailed measurements of all A_1 and E TO and LO phonons in the tetragonal BT were previously performed in single-domain crystals.[23]

According to the Raman tensor for the tetragonal C_{4v} point group, the α_{zz} component involves A_1 phonons exclusively. For the α_{xx} and α_{yy} components the A_1 and B_1 phonons are allowed simultaneously, while E modes are only allowed for α_{zx} and α_{zy} components. Consequently, in a perfect c-domain BST-x film the E_{TO} component of the soft mode can be observed in distinct scattering geometry. In the present work we used the so-called ''side-view backscattering'' geometry[36] that allows one to record pure A_1 and E modes from a c-domain tetragonal film using a micro-Raman setup. The wave vector of the incident light was parallel to the substrate while polarization of the incident/scattered light was parallel or perpendicular to the c axis of the film. As one can see in Fig. 1 the MgO substrate has no noticeable Raman lines in the spectral range studied.

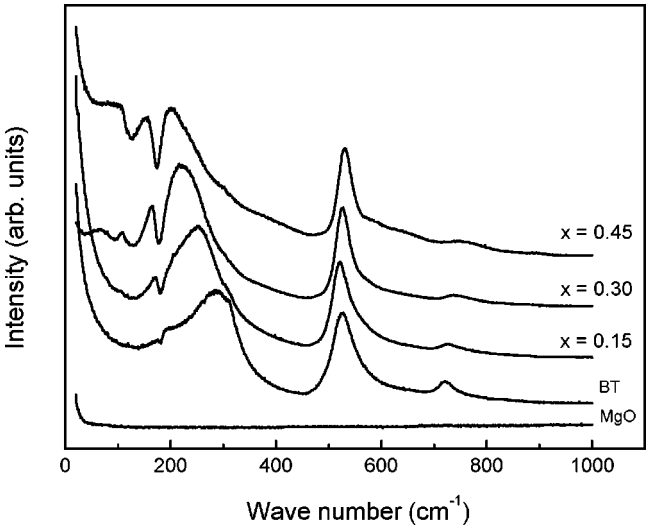

FIG. 1. Room temperature Raman spectra of BST-x thin films for $Y(ZZ)\bar{Y}$ scattering geometry.

The room-temperature Raman spectra of BT and BST thin films are shown in Figs. 1–3. As a result of excellent single-crystal quality of all the films, their Raman spectra exhibit remarkable polarization dependence. This feature safely confirms the absence of 90° domains in our films. However, the presence of 180° domains causes partial depolarization of the incident/scattered light on the domain walls and, therefore, leakage of intense lines into the forbidden geometries can be expected. Figure 1 shows pure A_1 phonons, where LO and TO components can be observed simultaneously because of light scattering on the domain walls. It is noticeable that main typical features of BT single crystal[23] have been clearly

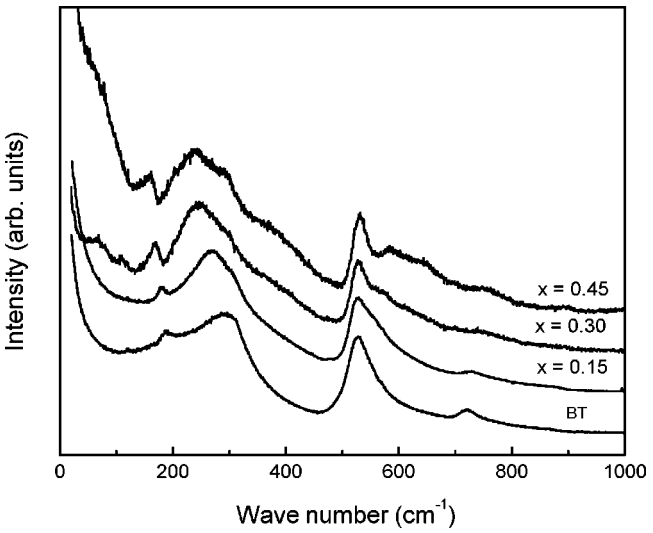

FIG. 2. Room temperature Raman spectra of BST-x thin films for $Y(XX)\bar{Y}$ scattering geometry.

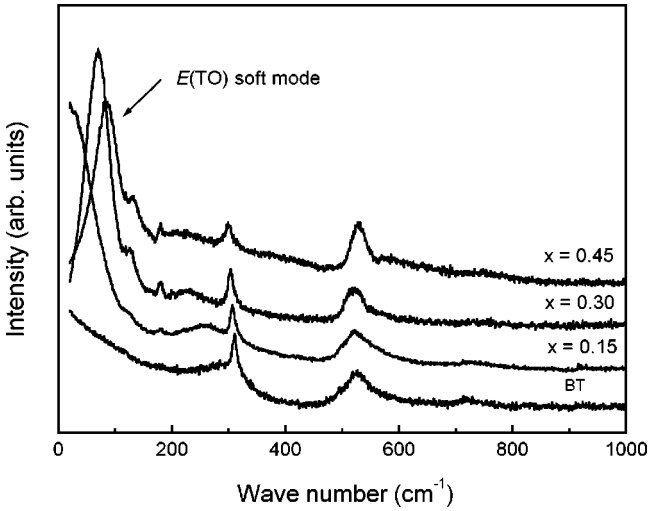

FIG. 3. Room temperature Raman spectra of BST-x thin films for $Y(XZ)\overline{Y}$ scattering geometry. The intensities have been corrected for the Bose-Einstein factor.

observed in the Raman spectra of the BT/MgO film. The sharp interference dip at 180 cm^{-1} and the broad peaks at 270, 525, and 720 cm^{-1} are remarkable characteristics of the $A_1(zz)$ spectrum of BT. In the xx spectrum (Fig. 2) the sharp dip apparently disappears and a narrow peak at $\sim$180 cm^{-1} emerges, as observed in BT single crystal. The E symmetry Raman spectrum contains the overdamped E_{TO} soft mode, which can be clearly seen in Fig. 3. Note that in this figure the intensities have been corrected for the temperature factor. The 180 cm^{-1} E mode is poorly resolved since it is overlapped with the tail of the overdamped soft mode in the BT film, but this peak is clearly seen in all BST films. As mentioned above, the cubic silent F_{2u} mode splits into B_1 and E components in the tetragonal phase. The corresponding E mode was observed at 308 cm^{-1} in the xz spectrum, whereas the B_1 component with nearly the same frequency can be traced in diagonal geometries. The high-frequency E modes at 466 (LO) and 489 (TO) cm^{-1} are rather weak even in the spectra of single crystals and in Fig. 3 these peaks are apparently overlapped with the broadband at 525 cm^{-1}. The latter peak, as well as the 270 cm^{-1} band, arise in the xz spectrum due to the leakage of the A_1 symmetry modes. In turn, the leakage of the E_{TO} soft mode into the diagonal geometries occurs.

All remarkable BT features dominate in the Raman spectra of the BST-x films presented in Figs. 1–3. Most of the peaks exhibit shifts with the increasing Sr content and additional bands centered at $\sim$380, 580, and 640 cm^{-1} arise in xx and zz spectra. The 130 cm^{-1} weak band overlapped with the tail of the soft mode was observed in the xz geometry. The most sensitive to the Ba/Sr substitution is the E_{TO} soft mode exhibiting remarkable upward shift with increasing x. Moreover, as can be seen in Fig. 3, this mode acquires underdamped line shape for $x \geqslant 0.3$. The E_{TO} frequencies and lattice parameters for all films studied are summarized in Table I. The broad peak observed at 280 cm^{-1} in BT and interpreted as $A_{1\,TO}$ component of the cubic F_{1u} soft mode exhibits considerable downward shift that makes the sharp

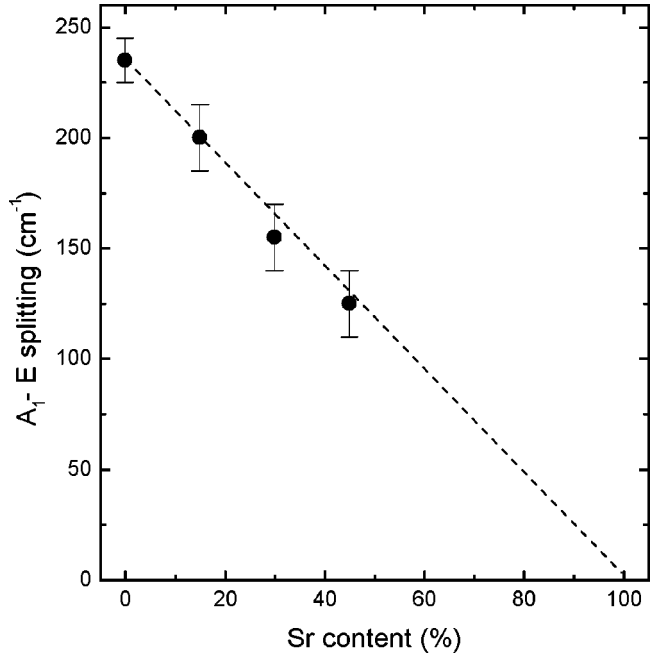

FIG. 4. A_1-E splitting of the soft mode as a function of the Sr content. The dashed line is a guide for the eye.

interference dip in zz spectra much more pronounced in BST-x films (see Fig. 1). To estimate the bare frequency of the $A_{1\,TO}$ soft mode we applied a coupled damped harmonic oscillator model to fit the experimental spectra obtained in zz geometry. The A_1-E splitting of the soft mode reflects the anisotropy of the short-range interatomic forces in the tetragonal phase. As shown in Fig. 4, the A_1-E splitting in BST-x films steadily decreases with increasing Sr concentration.

We have compared Raman spectra of BT and BST-0.3 ceramics with the aim to verify the soft-mode parameters in the bulk samples. Unpolarized Raman spectra of BT and BST-0.3 bulk ceramic samples at room temperature are shown in Fig. 5. Due to the random orientation of crystallites

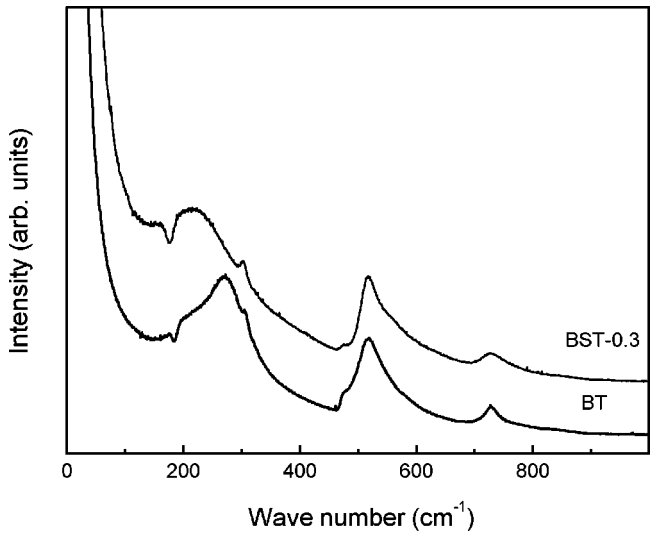

FIG. 5. Room temperature Raman spectra of BT and BST-0.3 ceramics.

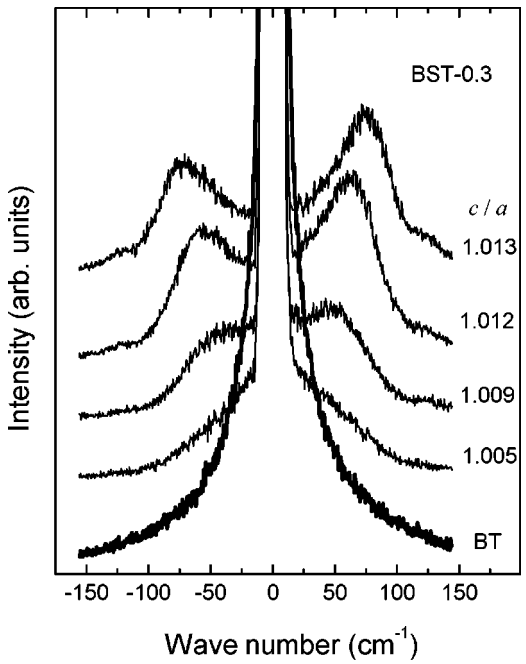

FIG. 6. E_{TO} soft mode in BST-0.3 films of different tetragonality. The overdamped soft mode in the BT film is shown for comparison.

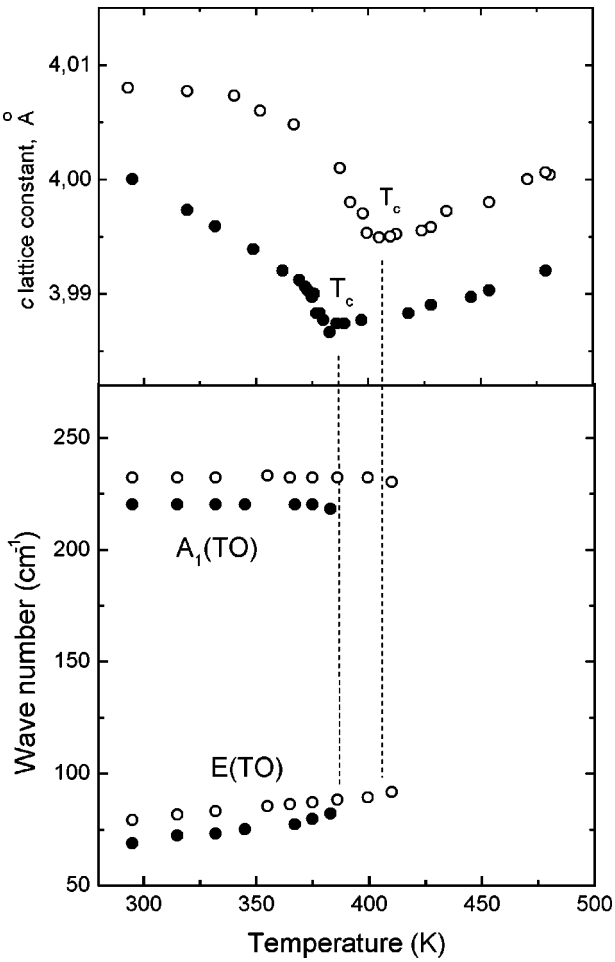

FIG. 7. Temperature dependence of the $A_{1\,TO}$ and E_{TO} components of the soft mode in BST-0.3 films near the ferroparaelectric phase transition. The upper panel shows temperature dependence of the unit-cell parameter. Open symbols correspond to the BST-0.3 film with $c/a=1.013$ at room temperature. Filled symbols correspond to the BST-0.3 film with $c/a=1.012$ at room temperature.

in a ceramic sample Raman bands of A_1 and E symmetry were obtained simultaneously. All remarkable features of bulk BT can be seen clearly and our spectra are very similar to those reported by Naik *et al.*[13] As shown in Fig. 5 the overdamped E_{TO} soft mode has practically the same shape in BT and BST-0.3 samples, whereas $A_{1\,TO}$ band exhibits a downward shift upon Sr addition. Comparing Figs. 1–3 and Fig. 5 one can conclude that the E_{TO} soft mode stiffness is a peculiar feature of heteroepitaxial thin films.

Varying the temperature of the substrate during the deposition we have obtained several BST-0.3 films of different tetragonality. As can be seen in Fig. 6, the lowest lying E_{TO} mode in these films is always underdamped with the maximum between 56 and 79 cm^{-1}. The tail of the overdamped soft mode in the BT film is shown in Fig. 6 for comparison (bold line). As one can see from Table I there is a strong correlation between the E_{TO} soft-mode frequency and the tetragonal distortion of the film.

Temperature dependence of the Raman spectra for BST-x films of different tetragonality and different composition was studied with the aim to the clarify temperature behavior of the E_{TO} and $A_{1\,TO}$ components of the soft mode at the ferroparaelectric phase transition. As in BT single crystals,[23,45] the frequency of the E_{TO} soft mode in BST-x films increases towards T_c, whereas frequency of the $A_{1\,TO}$ component is nearly constant. The temperature dependences for two selected BST-0.3 films of different tetragonality are shown in Fig. 7 together with the temperature dependencies of the unit cell parameter c in these films. The latter provides determination of T_c in thin films with a greater precision.

IV. DISCUSSION

A comparison of BT and BST-0.3 bulk ceramics at room temperature shows that in BST-0.3 the $A_{1\,TO}$ component of the soft mode is markedly shifted to lower wave numbers, while E_{TO} component remains overdamped and below 150 cm^{-1} both spectra are quite similar. Substitution of Ba by Sr with the smaller ionic radius causes local distortions and breaks partially the translational symmetry of the BT lattice. As a consequence the $\mathbf{q}=\mathbf{0}$ Raman selection rules are relaxed and activation of $\mathbf{q}\neq\mathbf{0}$ phonons from the Brillouin zone interior is expected in BST solid solutions. Accordingly, all Raman peaks in the spectra of BST-0.3 ceramics are slightly broadened and a new band near 580 cm^{-1} appears. Note that the latter peak emerges on the high-frequency shoulder of the 525 cm^{-1} band, which is markedly asymmetric in the spectrum of pure BT. The origin of the asymmetric line shape of this band in BT is not yet understood. To explain this asymmetry in the zz spectrum of pure BT crystals, Scalabrin *et al.*[23] introduced a coupling between the three A_1 modes and obtained perfect fitting curves. However, we agree with Burns and Dacol[45] that fitting procedure applied in Ref. 23 seems rather unphysical due to the very large coupling coefficients. It is rather doubtful that coupling be-

tween well-separated modes centered at ~270 and 525 cm^{-1} really occurs. One can assume that the remarkable asymmetry of the 525 cm^{-1} band is an intrinsic property of BT associated with the partial relaxation of the $\mathbf{q}=\mathbf{0}$ Raman selection rules due to the hopping motion of the Ti ions in the tetragonal phase. A comparison of BT and BST-0.3 bulk ceramics suggests that Ba/Sr substitution modifies the potential relief of the Ti ions and additional mode (or several modes) arises on the high-frequency asymmetrical shoulder of the 525 cm^{-1} band. We have to stress that the fitting of the BST-0.3 spectrum allows for one more component at about 620–640 cm^{-1}, but this component is rather weak and poorly defined to be included into consideration. An additional band at ~560 cm^{-1} was also observed in BST ceramics by Naik *et al.*,[13] moreover a weak feature near 620–640 cm^{-1} can be also traced in Fig. 2 of Ref. 13. Since unpolarized Raman spectrum contains all phonon modes, it is rather difficult to arrive at the final decision concerning this frequency range. Apparently, Raman spectra of heteroepitaxial thin films obtained in different scattering geometries are much more informative.

In the following, we consider a concentration dependence of the Raman spectra of thin films with the aim to identify normal modes, which are sensitive to the Ba/Sr substitution. Freire and Katiyar[20] have calculated the eigenvectors and the frequencies of each normal mode and reported graphical representation of all zone-center normal modes in the tetragonal phase of BT. According to the normal-mode classification, the soft mode in BT corresponds to a motion of the Ti ion against the oxygen octahedron. In the paraelectric phase the corresponding lowest-lying F_{1u} mode smoothly softens. Below T_c, the A_1 component becomes abruptly stable at ~270 cm^{-1}, whereas overdamped E component continues to soften from 60 cm^{-1} at T_c to 35 cm^{-1} at room temperature.[45] Apparently this mode is very sensitive to the change in the length of the Ti-O bond. The 180 cm^{-1} sharp line originates from the second F_{1u} IR active mode, which exhibits rather weak temperature dependence in the paraelectric phase.[24] This mode corresponds to a vibration of the Ba ions against the TiO_6 group. In the tetragonal phase the separation between the A_1 and E components of this mode is negligible; moreover, no LO-TO splitting was found in BT crystals.[23] In BST films this hard mode is practically unaltered upon Sr addition. The 308 cm^{-1} line originates from the silent F_{2u} mode, which exhibits neither B_1-E nor LO-TO splitting in the tetragonal phase.[23] The corresponding normal mode consists of out-of-phase vibrations of oxygens only. In BST films this mode shows no remarkable lifting in frequency with increasing Sr content. The third F_{1u} mode exhibits remarkable A_1-E splitting below T_c. Their LO and TO components are also well separated and in BT crystal $A_{1\,\mathrm{TO}}$ and $A_{1\,\mathrm{LO}}$ frequencies were found at 515 and 725 cm^{-1}, respectively.[23] This mode consists of a motion of the Ti and O1 ions against the O2 and O3 oxygens, which are located in the perpendicular plane, and is associated with a change in the Ti-O-Ti bond angle.

We have observed significant transformation of the A_1 and E components of the soft mode and activation of additional bands in the Raman spectra of heteroepitaxial BST thin films with respect to the bulk ceramics of the same composition. Moreover, from the ionic motion associated with each vibrational mode one can conclude that Sr incorporation seriously affects the Ti-O bonds in the host lattice. In the following discussion we consider three distinct phenomena that we assume to occur in thin films: (1) local lattice distortions due to Ba/Sr substitution; (2) oxygen vacancies; and (3) mechanical constraint imposed on the film by the underlying substrate.

Our results clearly show that the principal effect of Ba substitution by Sr in thin films is associated with a relatively large shift of the low-frequency Raman peaks attributed as E_{TO} and $A_{1\,\mathrm{TO}}$ components of the soft mode. The behavior of the soft-mode frequency in solid solutions is a result of a delicate balance among the short-range force constants, long-range interactions, and masses of the involved ions. The E_{TO} soft mode in BST films for $x \geqslant 0.3$ acquires the underdamped line shape, which is a remarkable characteristic of ST. Moreover, for a particular concentration ($x=0.3$) the E_{TO} eigenfrequency steadily increases with increasing c/a ratio. This behavior implies that the soft-mode hardening is not a simple mass effect of Ba/Sr substitution and indicates that the incorporation of Sr in the A sites deeply modifies the delicate balance of the short-range and long-range forces of BT lattice. A strong decrease in the A_1-E splitting of the soft mode with increasing Sr content suggests a reduction of the anisotropy of the short-range interatomic forces in BST films. Upon Sr addition, the spacing and bond angles between a particular atom and its second or third neighbors tend to be different. Being a microscopic technique, Raman spectroscopy is very sensitive to instantaneous atomic shifts from their regular sites. The directions of these displacements can be inferred from the Coulombic interactions with the neighboring atoms. Substitution of smaller Sr for Ba causes displacements of neighboring oxygens towards Sr and, consequently, leads to a decrease of the Ti-O-Ti bond angle. These distortions inevitably modify the short-range Ti-O force constants and disturb the Ti($3d$) and O($2p$) hybridization. As a consequence the phase-transition sequence in BST might be deeply modified.

For all BST films studied here the a parameter of the tetragonally distorted unit cell is smaller than that in bulk ceramics of the same composition. One can assume that decrease in the a parameter is associated with the decrease in the Ti-O-Ti bond angle making the Ti ions lying in basal plane closer to each other. The displacements from the time-averaged tetragonal positions and formation of a zigzag distortion of the Ti-O-Ti bonds change not only the soft-mode parameters, but may also cause appearance of new extra bands in the region of Ti-O vibrations at 580 and 640 cm^{-1}. Note, that these extra bands are much more pronounced in xx geometry than in the zz one (see Figs. 1 and 2), implying that the layer-by-layer growth makes the distorted Ti-O-Ti chains appear mostly in basal plane. Similar modes at ~560 and 620 cm^{-1} were also observed in BT powder samples under hydrostatic pressure beyond 2.1 GPa and were interpreted as caused by the shifts of the atoms from regular lattice sites to interstitial positions.[46] Note that extra bands at ~560 and 620 cm^{-1} were also observed in polycrystalline

BST films.[13] These authors concluded that the mode at $\sim 560\ \mathrm{cm}^{-1}$ is due to the disordered paraelectric phase, whereas the $620\ \mathrm{cm}^{-1}$ peak was attributed to the presence of enhanced grain boundaries in submicron-sized grains in thin films. In both cases these extra peaks are associated with the departure of the Ti ions from their regular sites in BT lattice. In the disordered cubic lattice the Ti ions occupy the body-centered positions on the average, though displaced along the cube diagonals and causing the disorder. The grain boundaries as well as domain walls are strongly distorted regions where profound alterations of the crystal structure compared to the bulk of the grains occur.

Furthermore, we have to take into account inevitable oxygen vacancies in films prepared by rf sputtering. It is important to realize that the atomic displacements around an oxygen vacancy also induce zigzag Ti-O-Ti chains. The nearest two Ti and four Ba cations are displaced away from the oxygen-vacancy defect while the nearest eight O anions are attracted towards it. Thus, both Sr and oxygen vacancies disturb Ti-O bonds and may have quite similar fingerprints in Raman response. The unit cell volumes of the films used in this study are very close to those of bulk ceramics. This fact suggests very low number of oxygen vacancies in our samples. Park and Chadi[47] have showed that oxygen vacancies in Ti-O-Ti chains along the polar c axis create local polar regions randomly distributed in the film volume. The number of oxygen vacancies plays a very important role in determining the dielectric properties of the film devices and their fatigue. A strong correlation between the dielectric properties of BST films and oxygen vacancy concentration has been recently reported.[48] Therefore, systematic studies on the influence of oxygen vacancies on the lattice dynamical properties of BST films are obviously required.

Enhanced tetragonal distortions in heteroepitaxial BST/MgO films arise also due to mechanical constraint imposed on the film by the substrate. There is a large lattice parameter mismatch between BST and MgO ($a_f < a_s$). Therefore, during the heteroepitaxial growth misfit dislocations appear to minimize the uncompensated energy of tensile stresses. As a result of this process, ''normalization'' of the unit cell parameters of the film occurs. However, BST/MgO thin films (thickness $<1\ \mu$m) exhibit considerable tetragonal distortion with respect to the bulk ceramics of the same composition. In heteroepitaxial BST films sputtered onto MgO(001) the thermoelastic compressive stresses ($\sigma_{11}=\sigma_{22}$) are generated by the mismatch of the thermal expansion coefficients of the film and substrate ($\alpha_f < \alpha_s$) and appear on cooling from the deposition temperature. These strong compressive stresses are minimized if, on cooling through the ferroelectric phase transition, the tetragonal unit cells appear with the c axis normal to the substrate surface. A tail-to-tail polarization is one of the patterns that emerges from atomic relaxations around oxygen vacancies.[47] Such vacancy-induced antiphase polarizations can play an important role in domain pinning in thin films on cooling from the deposition temperature. It is well known that in bulk crystals and large grain ceramics 90° and 180° domains appear to minimize elastic and electrostatic energies in the tetragonal ferroelectric state. Therefore, bulk materials are usually fully transformed and essentially unstressed. The long-range nature of the forces involved in ferroelectric transition and the large electrostatic energies driving domain formation suggest that the size effects are very important in thin films. Strong compressive stresses and inevitable oxygen vacancies lead to the specific 180° domain structure in BST films prepared on MgO.

In our films the value $\sigma_{11}=\sigma_{22}$ was estimated from XRD measurements to be in the range 200–450 MPa at room temperature. Since the two-dimensional (2D) stresses are higher in films with larger c/a ratio, one can assume that these strong compressive stresses result in an enhanced tetragonal distortion of the film. These additional distortions give rise to Raman bands, which would be normally forbidden for the undistorted tetragonal lattice. Uwe *et al.*[49] have shown that a nonzero Raman intensity is expected to arise due to the coupling of normal modes with the static distortion. A large part of the Brillouin zone will contribute to the scattering and the intensity of these modes is proportional to the Fourier transform of the static distortion. Thus, the observed broadening of the Raman lines in BT film with regard to the single crystal reflects the effect of the strain field. Beside the coupling of the normal modes with the static distortion the $\mathbf{q}=\mathbf{0}$ Raman selection rules are relaxed due to breaking of the translational symmetry in BST solid solution and at the moment we are unable to separate these effects. Adequate quantitative estimations call for polarized Raman spectra obtained from epitaxial films and single crystals under the same experimental conditions.

As shown above, Ba/Sr substitution induces a relatively large shift of the soft-mode components in BST films. Besides, the soft mode must be very sensitive to the biaxial constraint imposed by the substrate. It is known that 2D compressive stress results in an increase in the cubic-tetragonal transition temperature, while a decrease is expected for hydrostatic pressure.[4,50] Accordingly, under hydrostatic pressure the soft mode exhibits a downward shift, whereas an upward shift is expected under in-plane 2D compressive stress. As it is shown in Fig. 6 the E_{TO} soft-mode frequency increases from 56 to $79\ \mathrm{cm}^{-1}$ with increasing c/a ratio. The 2D compressive stress also increases from 200 to 450 MPa with increasing c/a ratio. The tetragonality of the all BST-0.3 films was found larger (see Table I) than that of bulk ceramics of corresponding composition (bulk $c/a=1.003$). However, the unit-cell volumes of these films are nearly equal to that of bulk samples, implying that the distortion of the BST-x films is in agreement with the Poisson ratio. This fact also suggests that our BST-0.3 films exhibit very low concentration of oxygen vacancies, which have to increase the unit-cell volume due to reduction of the Coulomb attractive forces. Therefore, one can conclude that the observed E_{TO} soft-mode hardening in BST-0.3 films is mostly associated with the 2D compressive stress.

From the temperature dependence of the lattice parameters we have found that T_c exhibits upward shift in BST-0.3 films in agreement with Landau-Devonshire theory.[4,50] Moreover, due to the significant 2D clumping and inevitable point defects the ferroparaelectric phase transition in thin films is usually diffuse. In thin ferroelectric films dielectric susceptibility usually exhibits rather broad peak and tem-

perature dependence of the lattice constants is also rather smooth. It is difficult to indicate the transition point but rather the transition interval (usually 10–20 K) where $c(T)$ curve exhibits smooth minima and domain patterns (observed using scanning electron microscopy) disappear. For BST-0.3 films studied in this work T_c increases from 360 ± 5 K up to 400 ± 5 K with increasing 2D compressive stress from 200 to 450 MPa (c/a ratio increases from 1.005 to 1.013, respectively). As in BT single crystals,[23,45] the frequency of the E_{TO} soft mode increases gradually on approaching T_c from below. The linewidth also increases but the soft modes in BST-0.3 and BST-0.45 films are always underdamped. A typical frequency shift of the underdamped E_{TO} soft mode never exceeds 12 ± 3 cm^{-1} in the temperature interval 295–420 K. The frequency of the $A_{1\,\mathrm{TO}}$ component of the soft mode is practically temperature independent. No discontinuity was observed near T_c in agreement with the diffuse character of the ferroparaelectric transition. Above T_c all Raman peaks steadily lose their intensity but several broad features persist far beyond T_c as well as in BT single crystals.

Therefore, the decrease in the A_1-E splitting with increasing Sr content is much more pronounced with respect to the temperature variation of this splitting near T_c. Actually, error bars in Fig. 4 include temperature evolution of the E_{TO} component of the soft mode in the whole temperature range from room temperature up to T_c.

V. CONCLUSIONS

Polarization-dependent Raman spectra of heteroepitaxial BST-x ($x=0$, 0.15, 0.30, and 0.45) prepared on MgO substrates were obtained in ''side-view backscattering'' geometry. It is found that all remarkable BT features dominate in the Raman spectra of the BST-x films. We assume that Sr incorporation in the A sites modifies the short-range and long-range forces of BT lattice and causes local distortions of the Ti-O-Ti chains. As a consequence, several additional bands at 130, 380, 580, and 640 cm^{-1} arise in the Raman spectra with increasing Sr content. The most sensitive to the Ba/Sr substitution is the E_{TO} soft mode that exhibits remarkable hardening with increasing x and acquires underdamped line shape for $x \geqslant 0.3$. A strong decrease in the A_1-E splitting of the soft mode with increasing Sr content suggests a reduction of the anisotropy of the short-range interatomic forces in BST films. It is shown that E_{TO} soft mode is also very sensitive to the mechanical constraint imposed on the film by the substrate.

As in pure BT crystal, the frequency of the E_{TO} soft mode increases on approaching T_c from below, whereas the $A_{1\,\mathrm{TO}}$ component of the soft mode is temperature independent. Both Raman and XRD measurements confirmed upward shift of T_c in BST-0.3 films, as expected from a conventional Landau-Devonshire approach.[4,50]

ACKNOWLEDGMENTS

Helpful discussions with J. Petzelt and I. Gregora are gratefully acknowledged. We thank S. I. Shevtsova for performing primary x-ray characterization and A. Costa for technical assistance. This work was partially supported by the Russian Foundation for Basic Research (Grant No. 98-02-18069), and also by the projects PRAXIS XXI/3/3.1/MMA/1769/95 and PRAXIS/P/FIS/14287/1998. Yuri Yuzyuk thanks Projecto PRAXIS XXI for his grant BCC/4463/96.

[1] J.F. Scott, Ferroelectr. Rev. **1**, 1 (1998); S. R. Summerfelt, in *Ferroelectric Thin Films*, edited by R. Ramesh (Kluwer Academic, Netherlands, 1997), Chap. 1, p. 1.

[2] A.I. Kingon, S.K. Streiffer, C. Basceri, and S.R. Summerfelt, Mater. Res. Bull. **21**, 46 (1996); F. Jin, G.W. Auner, R. Naik, N.W. Schubring, J.V. Mantese, A.B. Catalan, and A.L. Micheli, Appl. Phys. Lett. **73**, 2838 (1998).

[3] J.S. Horwitz, W. Chang, A.C. Carter, J.M. Pond, S.W. Kirchoefer, D.B. Chrisey, J. Levy, and C. Hurbert, Integr. Ferroelectr. **22**, 799 (1998).

[4] I.N. Zakharchenko, E.S. Nikitin, V.M. Mukhortov, Yu.I. Golovko, M.G. Radchenko, and V.P. Dudkevich, Phys. Status Solidi A **114**, 559 (1989).

[5] B.A. Baumert, L.-H. Chang, A.T. Matsuda, T.-L. Tsai, C.J. Tracy, R.B. Gregory, P.L. Fejes, N.G. Cave, W. Chen, D.J. Taylor, T. Otsuki, E. Fujii, S. Hayashi, and K. Suu, J. Appl. Phys. **82**, 2558 (1997).

[6] S.K. Streiffer, C. Basceri, C.B. Parker, S.E. Lash, and A.I. Kingon, J. Appl. Phys. **86**, 4665 (1999).

[7] W. Chang, C.M. Gilmore, W.-J. Kim, J.M. Pond, S.W. Kirchoefer, S.B. Qadri, D.B. Chirsey, and J.S. Horwitz, J. Appl. Phys. **87**, 3044 (2000).

[8] I. Taguchi, A. Pignolet, L. Wang, M. Proctor, F. Levy, and P.E. Schmid, J. Appl. Phys. **73**, 394 (1993).

[9] L.H. Robins, D.L. Kaiser, L.D. Rotter, P.K. Schenck, G.T. Stauf, and D. Ritz, J. Appl. Phys. **76**, 7487 (1994).

[10] Yu.I. Yuzyuk, R. Farhi, V.L. Lorman, L.M. Rabkin, L.A. Sapozhnikov, E.V. Sviridov, and I.N. Zakharchenko, J. Appl. Phys. **84**, 452 (1998).

[11] P.S. Dobal, S. Bhaskar, S.B. Majumder, and R.S. Katiyar, J. Appl. Phys. **86**, 828 (1999).

[12] A.A. Sirenko, I.A. Akimov, J.R. Fox, A.M. Clark, H.-C. Li, W. Si, and X.X. Xi, Phys. Rev. Lett. **82**, 4500 (1999).

[13] R. Naik, J.J. Nazarko, C.S. Flattery, U.D. Venkateswaran, V.M. Naik, M.S. Mohammed, G.W. Auner, J.V. Mantese, N.W. Schubring, A.L. Micheli, and A.B. Catalan, Phys. Rev. B **61**, 11367 (2000).

[14] I. Fedorov, V. Železný, J. Petzelt, V. Trepakov, M. Jelinek, V. Trtik, M. Čerňanský, and V. Studnička, Ferroelectrics **208-209**, 413 (1998).

[15] A.A. Sirenko, C. Bernhard, A. Golnik, A.M. Clark, J. Hao, W Si, and X.X. Xi, Nature (London) **404**, 373 (2000).

[16] M.E. Lines and A.M. Glass, *Principles and Applications of Ferroelectrics and related Materials* (Clarendon, Oxford, 1977), p. 680.

[17] K.-H. Weyrich and R. Siems, Z. Phys. B: Condens. Matter **61**, 63 (1985).
[18] R.E. Cohen and H. Krakauer, Phys. Rev. B **42**, 6416 (1990).
[19] R. Comes, M. Lambert, and A. Guinier, Solid State Commun. **6**, 715 (1968).
[20] J.D. Freire and R.S. Katiyar, Phys. Rev. B **37**, 2074 (1988).
[21] A.V. Turik and A.G. Khasabov, J. Phys.: Condens. Matter **10**, 2477 (1998).
[22] M.P. Fontana and M. Lambert, Solid State Commun. **10**, 1 (1972).
[23] A. Scalabrin, A.S. Chaves, D.S. Shim, and S.P.S. Porto, Phys. Status Solidi B **79**, 731 (1977).
[24] Y. Luspin, J.L. Servoin, and F. Gervais, J. Phys. C **13**, 3761 (1980).
[25] H. Vogt, J.A. Sanjurjo, and G. Rossbroich, Phys. Rev. B **26**, 5904 (1982).
[26] J. Petzelt, G.V. Kozlov, and A.A. Volkov, Ferroelectrics **73**, 101 (1987).
[27] K. Laabidi, M.D. Fontana, and B. Jannot, Solid State Commun. **76**, 765 (1990).
[28] J.L. Servoin, Y. Luspin, and F. Gervais, Phys. Rev. B **22**, 5501 (1980).
[29] Y. Yamada and G. Shirane, J. Phys. Soc. Jpn. **26**, 396 (1969).
[30] P.A. Fleury and J.M. Worlock, Phys. Rev. **174**, 613 (1968).
[31] A.D. Bruce, K.A. Muller, and W. Berlinger, Phys. Rev. Lett. **42**, 185 (1979).
[32] V.V. Lemanov, Phys. Solid State **39**, 318 (1997).
[33] D. Louca, H. Roder, J.L. Sarrao, D.A. Dimitrov, J.M. Wills, P.S. Swart, and A.R. Bishop, J. Phys. Chem. Solids **61**, 239 (2000).
[34] F. Gervais, J.L. Servoin, and B. Jannot, Ferroelectr. Lett. Sect. **2**, 161 (1984).
[35] V. Železný, J. Petzelt, and K. Krammer, J. Korean Phys. Soc. **32**, S1615 (1998).
[36] Yu.I. Yuzyuk, A. Almeida, M.R. Chaves, V.A. Alyoshin, I.N. Zakharchenko, and E.V. Sviridov, Phys. Status Solidi B **222**, 535 (2000).
[37] J. Petzelt, T. Ostapchuk, S. Kamba, I. Rychetský, M. Savinov, A. Volkov, B. Gorshunov, A. Pronin, S. Hoffmann, R. Waser, and J. Linder, Ferroelectrics **239**, 987 (2000).
[38] J. Petzelt, T. Ostapchuk, S. Kamba, in *Defects and Surface-induced Effects in Advanced Perovskites*, Vol. 77 of NATO Science Series 3: High Technology, edited by G. Borstel *et al.* (Kluwer Academic, Netherlands, 2000), p. 233.
[39] J. Petzelt and T. Ostapchuk, Ferroelectrics **249**, 81 (2001).
[40] J. Petzelt, T. Ostapchuk, S. Kamba, I. Gregora, I. Rychetský, J. Pokorný, V. Bovtun, V. Porokhonsky, M. Savinov, S. Hoffmann, R. Waser, and J. Linder, Integr. Ferroelectr. **32**, 11 (2001).
[41] V.M. Mukhortov, Yu.I. Golovko, V.A. Alyoshin, E.V. Sviridov, Vl.M. Mukhortov, and V.P. Dudkevich, Phys. Status Solidi A **78**, 253 (1983).
[42] Z. Surowiak, Y.S. Nikitin, S.V. Biryukov, Yu.I. Golovko, V.M. Mukhortov, and V.P. Dudkevich, Thin Solid Films **208**, 76 (1992).
[43] V.A. Alyoshin, E.V. Sviridov, Vl.M. Mukhortov, I.N. Zakharchenko, and V.P. Dudkevich, in *Ferroelectric Thin Films IV*, edited by S.B. Desu *et al.*, Mater. Res. Soc. Symp. Proc. No. 361 (Material Research Society, Pittsburg, 1995), p. 501.
[44] V.A. Alyoshin, E.V. Sviridov, I.N. Zakharchenko, and V.P. Dudkevich, Radiat. Eff. Defects Solids **134**, 321 (1995).
[45] G. Burns and F.H. Dacol, Phys. Rev. B **18**, 5750 (1978).
[46] U.D. Venkateswaran, V.M. Naik, and R. Naik, Phys. Rev. B **58**, 14 256 (1998).
[47] C.H. Park and D.J. Chadi, Phys. Rev. B **57**, R13 961 (1998).
[48] W.J. Kim, W. Chang, S.B. Qadri, J.M. Pond, S.W. Kirchoefer, D.B. Chrisey, and J.S. Horwitz, Appl. Phys. Lett. **76**, 1185 (2000).
[49] H. Uwe, K.B. Lyons, H.L. Carter, and P.A. Fleury, Phys. Rev. B **33**, 6436 (1986).
[50] G.A. Rossetti, Jr., L.E. Cross, and K. Kushida, Appl. Phys. Lett. **59**, 2524 (1991).